JGR Space Physics

RESEARCH ARTICLE
10.1029/2024JA033504

A New Electron and Proton Radiation Belt Identified by CIRBE/REPTile-2 Measurements After the Magnetic Super Storm of 10 May 2024

Xinlin Li[1,2], Zheng Xiang[1], Yang Mei[1,2], Declan O'Brien[1,2], David Brennan[1], Hong Zhao[3], Daniel N. Baker[1], and Michael A. Temerin[4]

[1]Laboratory for Atmospheric and Space Physics, University of Colorado Boulder, Boulder, CO, USA, [2]Department of Aerospace Engineering Sciences, University of Colorado Boulder, Boulder, CO, USA, [3]Department of Physics, Auburn University, Auburn, AL, USA, [4]Retired from Space Sciences Lab, UC Berkeley, Berkeley, CA, USA

Key Points:

- Two new radiation belts: 1.3–5 MeV electrons at $L \sim 2.5$–3.5 and 6.8–20 MeV protons at $L \sim 2$, were identified following the 5/10/2024 storm
- The long-lasting nature of the belts has physical implications for wave-particle interactions (electrons) and collisional loss (protons)
- Detailed spectrum of the new electron belt was revealed due to the high-energy-resolution of REPTile-2

Correspondence to:
X. Li,
Xinlin.Li@lasp.colorado.edu

Citation:
Li, X., Xiang, Z., Mei, Y., O'Brien, D., Brennan, D., Zhao, H., et al. (2025). A new electron and proton radiation belt identified by CIRBE/REPTile-2 measurements after the magnetic super storm of 10 May 2024. *Journal of Geophysical Research: Space Physics*, *130*, e2024JA033504. https://doi.org/10.1029/2024JA033504

Received 5 NOV 2024
Accepted 9 JAN 2025

Author Contributions:
Conceptualization: Xinlin Li, Declan O'Brien, Hong Zhao, Daniel N. Baker, Michael A. Temerin
Formal analysis: Xinlin Li, Zheng Xiang, Yang Mei
Funding acquisition: Xinlin Li
Investigation: Xinlin Li, Zheng Xiang, Hong Zhao, Michael A. Temerin
Methodology: Xinlin Li, Zheng Xiang, Yang Mei
Project administration: Xinlin Li
Resources: Xinlin Li
Software: Zheng Xiang, Yang Mei, Declan O'Brien
Supervision: Xinlin Li, Daniel N. Baker
Validation: Zheng Xiang, Yang Mei, Declan O'Brien
Writing – original draft: Xinlin Li, Zheng Xiang, Yang Mei, Declan O'Brien, Michael A. Temerin

Abstract Following the largest magnetic storm in 20 years (10 May 2024), REPTile-2 on NASA's CIRBE satellite identified two new radiation belts containing 1.3–5 MeV electrons around $L = 2.5$–3.5 and 6.8–20 MeV protons around $L = 2$. The region around $L = 2.5$–3.5 is usually devoid of relativistic electrons due to wave-particle interactions that scatter them into the atmosphere. However, these 1.3–5 MeV electrons in this new belt seemed unaffected until a magnetic storm on 28 June 2024, perturbed the region. The long-lasting nature of this new electron belt has physical implications for the dependence of electron wave-particle interactions on energy, plasma density, and magnetic field strength. The enhancement of protons around $L = 2$ exceeded an order of magnitude between 6.8 and 15 MeV forming a distinct new proton belt that appears even more stable. CIRBE, after a year of successful operation, malfunctioned 25 days before the super storm but returned to functionality 1 month after the storm, enabling these discoveries.

Plain Language Summary Energetic electrons with energies ranging from hundreds of keV to over multiple MeV, along with protons exceeding multiple MeV, pose significant risks to spacecraft systems and astronauts during spacewalks. These particles in the near-Earth environment are known to exhibit substantial variations, particularly during geomagnetic storms, which are triggered by solar flares and coronal mass ejections from the Sun. Following the most intense magnetic storm in 20 years on 10 May 2024, NASA's CIRBE (Colorado Inner Radiation Belt Experiment) CubeSat identified two new radiation belts using its high-resolution REPTile-2 (Relativistic Electron and Proton Telescope integrated little experiment-2) science payload. One belt contained electrons with energies between 1.3 and 5 MeV located around $L = 2.5$–3.5 (L represents the geocentric distance in Earth radii at the equator from Earth's center of the magnetic field line). The other belt contained protons with energies between 6.8 and 20 MeV located around $L = 2$. The long-lasting nature of these belts provides insights into wave-particle interactions, including information about the electron belt's lifetime and energy loss processes affecting the new proton belt through atmospheric collisions.

1. Introduction

Earth's electron radiation belts usually consist of two distinct zones: the inner belt, centered near $L = 1.5$ (L is a dimensionless parameter describing the magnetic shell that represents the geocentric distance in Earth radii (R_E) at the equator of the shell) and the outer radiation belt which is most intense around $L = 4$ and 5. The slot region, where few energetic electrons dwell, separates the two radiation belts. The inner belt ($L < 2$) also contains protons with energies of multiple MeV to GeV (e.g., W. Li & Hudson, 2019; X. Li & Temerin, 2001). A month after the super storm of 10 May 2024, where the Disturbance storm-time index (Dst) reached ∼−400 nT, a new electron belt containing 1.3–5 MeV electrons around $L = 2.5$–3.5 and a new proton belt containing 6.8–20 MeV protons around $L = 2$ was measured by REPTile-2 (Relativistic Electron and Proton Telescope integrated little experiment-2), the sole science payload on CIRBE (Colorado Inner Radiation Belt Experiment), a three-unit CubeSat that was launched on 15 April 2023 into a sun synchronous orbit (97.4° inclination and 509 km altitude) with its ascending local time at ∼10:30 a.m. REPTile-2 includes a stack of four silicon detectors (D1, D2, D3, and D4) of the same size. Each detector is separated into an inner area and outer ring (inner diameter: 20 mm; outer diameter: 40 mm), which is also known as guard ring. The guard rings are used in anti-coincidence, such that a trigger of the outer area would veto the event. Only events, which come in from the instrument's field of view (FOV), that trigger the inner areas of detectors D1, D1 + D2, D1 + D2 + D3, and D1 + D2 + D3 + D4 are counted as valid.

Writing – review & editing: Xinlin Li, Michael A. Temerin

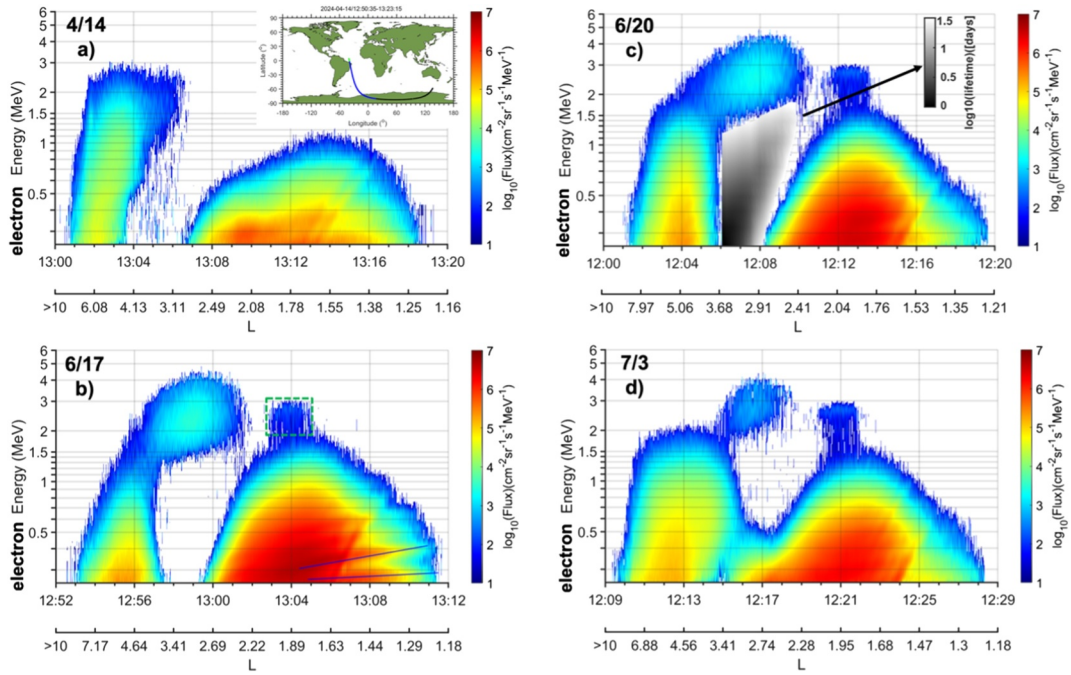

Figure 1. Color-coded logarithmic electron fluxes as a function of time and energy, accompanied by a secondary *x* axis showing the corresponding *L*, during a pass through the center of the SAA on four different dates as labeled. A small map indicating CIRBE's pass on 4/14 is inserted in (a). The fluxes inside the dashed green square at $L \sim 2$ in (b), and visible in (c) and (d), are contamination by 6.5–7 MeV protons, see Figure 2. A diagram showing calculated lifetimes due to interaction with plasma hiss waves is inserted in (c). Drift echoes or zebra stripes in the inner belt are visible in (b), indicated by the two solid blues lines. CIRBE's altitude is decreasing, at ∼436.3 km on 6/17, ∼434.5 km on 6/20, and ∼428.9 km on 7/3 when passing through $L \sim 3$. The effects of the altitude are discussed in Section 3.3.

This anticoincidence logic eliminates contaminations from side penetrating highly energetic particles (mostly >∼60 MeV protons). The inner area signals are passed to pulse height analyzers. The pulse-height-analysis technique incorporated by REPTile-2 instrument enables 60 electron energy channels (0.25–6 MeV) and 60 proton channels (6.5–100 MeV) at a cadence of 1 s (Khoo et al., 2022; X. Li, 2024; X. Li, Selesnick, et al., 2024; X. Li et al., 2022). CIRBE was delayed in identifying the new radiation belts because it suffered an anomaly on 15 April 2024 (after working well for a year) and only resumed its normal science mode on 16 June 2024. Thanks to the high-energy-resolution measurements of REPTile-2, the new electron belt and proton belt were immediately obvious.

2. Observations

Figure 1 shows the electron fluxes derived from the least-squares inversion method (Khoo et al., 2022; Selesnick et al., 2018; Tarantola, 2005; Tarantola & Valette, 1982) from REPTile-2 measurements during four similar passes through the center of the South Atlantic Anomaly (SAA) on four different dates in 2024, as labeled. These electrons are mostly trapped. A small map with the CIRBE track is inserted on Figure 1a (4/14). Color-coded electron differential fluxes are plotted versus time (and L as the secondary *x*-axis). Structure of two belts and a slot region is evident on 4/14, 1 day before CIRBE went silent and ∼4 weeks before the super storm.

On 6/17 (Figure 1b), the outstanding new feature is the new electron radiation belt with energy between 1.3 and 5 MeV around $L = 3$. Also outstanding is that there are no measurable electrons with energies below 1.3 MeV in that region. Additionally, the electron flux in the inner belt is much higher with clear enhancements of >1.5 MeV electrons and more structures are visible, such as zebra stripes (guided by the blue lines) (e.g., X. Li, Selesnick, et al., 2024; Mei et al., 2025). The outer belt electron flux has changed as well, with more lower energy electrons and fewer high energy electrons. Electron fluxes based on REPTile-2 measurements during a similar pass on 6/20 are displayed on Figure 1c, in which a diagram showing calculated lifetimes (gray-color-coded, as a function of energy and *L*), due to interaction with plasma hiss waves, of the electrons ranging from 100 s of keV to multiple

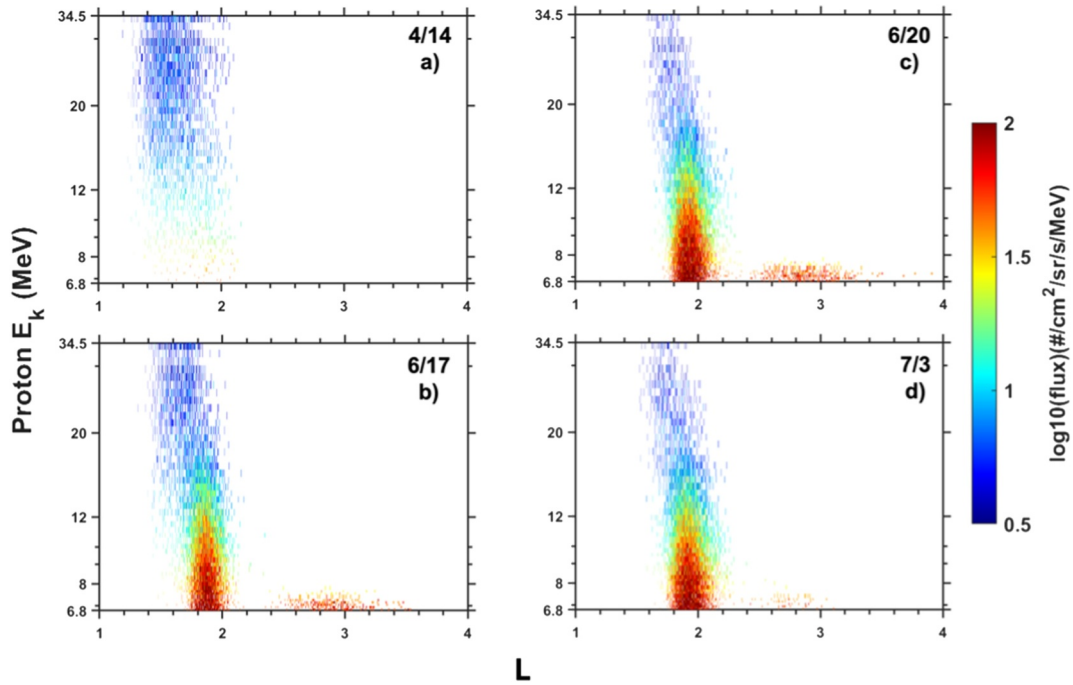

Figure 2. Color-coded logarithmic proton fluxes as a function of time and L, during the same passes as in Figure 1. The low energy protons, 6.8–7.5 MeV, at $L > 2.3$, are contaminated by >∼3 MeV electrons (Khoo et al., 2022).

MeV that have filled the empty region right after the storm was inserted (Pierrard et al., 2024), providing an explanation of why the new belt contains only highly energetic electrons (1.3–5 MeV) around $L \sim 2.5$–3.5 (see discussions in the next Section).

Figure 1d shows electron fluxes based on REPTile-2 measurements during a similar pass on 7/3, following a magnetic storm that occurred on 6/28 (Dst ∼ −80 nT, see Figure 3). The electron flux remained almost the same in the inner belt but changed significantly elsewhere, including the new electron belt (1.3–5 MeV), which decayed significantly but was still visible.

Figure 2 shows the proton measurements for the same four passes as in Figure 1. Before the super storm, the inner belt protons are shown in Figure 2a. The new proton belt is obvious after the superstorm, as shown in Figures 2b–2d. The new proton belt formed at $L < 2.2$, seems more stable and was not affected by the storm that occurred on 6/28, see the bottom panel (Dst index) of Figure 3. Previous studies suggest that radiation belt protons at $1.7 < L < 2.3$ vary gradually on time scales of ∼1 year (Albert & Ginet, 1998; Selesnick et al., 2016). The loss of radiation belt protons is mainly due to collisions with free electrons, bound electrons, and nuclei in the ambient plasma and neutral atmosphere (Albert et al., 1998; Selesnick et al., 2007). Collisions with free and bound electrons produce energy losses that are stronger than nuclear scattering. Protons at larger L will experience more rapid changes caused by field line curvature scattering (Selesnick & Looper, 2023; Selesnick et al., 2016; Young et al., 2002), which breaks the first adiabatic invariant of a proton and leads to pitch angle diffusion (Young et al., 2008). There are two parameters: the ratio of the locally mirroring proton gyroradius to the radial magnetic field gradient scale length (ε), and the ratio of the distance traveled along the magnetic field line in a gyro period to the radius of curvature (η) (Engel et al., 2016; Z. Li et al., 2024). Typically, $\varepsilon > 0.1$ is considered to represent the onset of nonadiabatic motion (Sergeev & Tsyganenko, 1982; Tu et al., 2014), leading to loss by cumulative field line curvature scattering. However, for the new belt protons (6.8–15 MeV) at L around 2, the corresponding ε values are <0.05. Thus, we expect that the new proton belt will last for many months, perhaps over a year.

To put things in context, we show POES-18 measurements of integral electron fluxes from the 90° telescope (Evans & Greer, 2004) and the predicted Dst and Auroral Electrojet (AE) indices (X. Li et al., 2007; Luo et al., 2013; Temerin & Li, 2006) between 4/14 and 7/5 of 2024 in Figure 3. The super storm started on May 10, leading to the enhancement and deep penetration of energetic electrons to lower L. Some electrons were driven

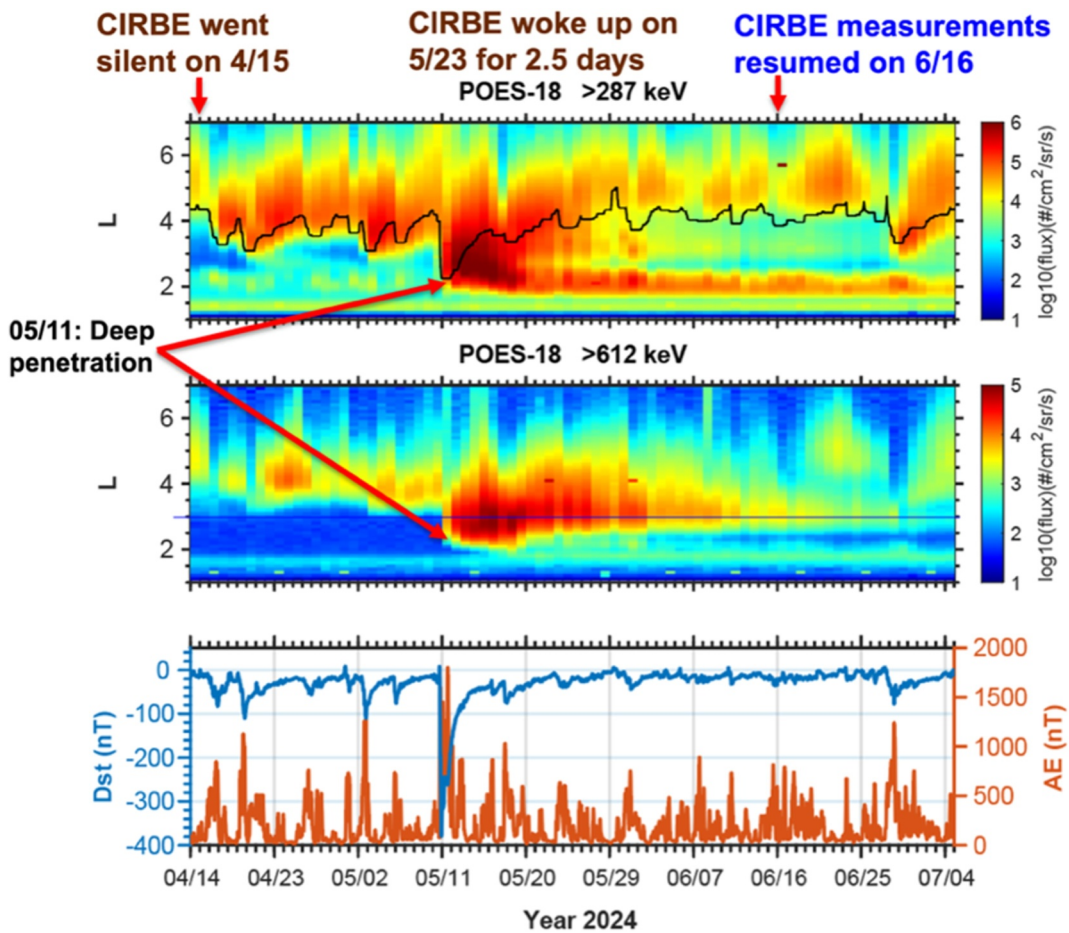

Figure 3. Daily averaged integral electron fluxes measured by POES-18, with timelines of CIRBE stated on the top, for integral channels >287 and >612 keV, and Dst and AE indices (predicted). The black curve on the first panel is calculated plasmapause location based on an empirical formula (O'Brien & Moldwin, 2003). The thin blue line on panel 2 indicates $L = 3$.

into the inner belt as well, which is a common occurrence associated with a major magnetic storm (e.g., Baker et al., 2004; X. Li et al., 1999). Here we focus on the region around $L = 3$ for the electrons, guided by the thin blue line (in the 2nd panel), where few energetic electrons dwelled before the storm. After the super storm, the integral electron fluxes appear to decrease in this region. By the time CIRBE resumed measurements on 6/16, some >612 keV electrons are still visible in that region ($L = 3$), in the 2nd panel. However, REPTile-2 revealed that these electrons are between 1.3 and 5 MeV, as shown in Figures 1b and 1c: not 700 keV or 800 keV, or any electrons below 1.3 MeV in that region. There are recorded counts in the lower energy channels of REPTile-2 as well. However, calculating the flux using a least-squares inversion method, which accounts for REPTile-2's full instrument response functions (Khoo et al., 2022; Selesnick et al., 2018; Tarantola, 2005; Tarantola & Valette, 1982), we determine that these counts in the lower energy channels are contributed by high energy (>1.3 MeV) electrons. Thus, we conclude there are no lower energy (<1.3 MeV) electrons in the new belt after CIRBE/REPTile-2 resumed operation (6/16 onward). This demonstrates that having high-energy-resolution measurements is critical. The new electron belt could not have been correctly identified from such integral flux measurements alone. Based on PROBA-V/EPT measurements, which has six channels between 0.5 and 8 MeV, Pierrard et al. (2024) showed the continuous temporal evolution of the electron fluxes before, during, and after the super storm, see Figure 7 of Pierrard et al. (2024). They identified a new electron belt located between $L = 2.5$ and $L = 4$ but they did not discuss the different decay rate for different energy electrons in the new electron belt. REPTile-2, with 60 channels between 0.25 and 6 MeV electrons, reveals more detailed energy dependence of

the new belt electrons, providing a good opportunity to discuss interactions between the electrons and plasma hiss waves (next section).

3. Discussion

3.1. Unique Features of Dynamic Variations of Radiation Belt Electrons Associated With This Super Magnetic Storm

The remnant belts of MeV electrons were previously reported using observations from the Van Allen Probes (Baker et al., 2013, 2019). There are several differences between the new belts observed by CIRBE and the remanent belts observed by the Van Allen Probes.

1. Forming mechanism. During the 10 May 2024 storm, the enhancements of relativistic electrons occurred through a wide L range, down to $L < 2$ (inner belt), based on POES measurements and PROBA-V/EPT measurements (Pierrard et al., 2024). It is our understanding that the lower energy (<1.3 MeV) electrons were scatted by hiss waves in the slot region ($L = 2.5$–3.5) and left >1.3 MeV electrons as the remnant belt. During the 2 September 2012 storm, the pre-existing >2 MeV electrons experienced slight penetration processes due to the moderate activity (the minimal Dst index is around −70 nT). The outer part of the outer belt was depleted by the magnetopause shadowing to form the remnant belts. There are no >2 MeV electrons observed at $L < 2.8$ and no >1 MeV electrons observed at $L < 1.5$ by Van Allen Probes during their entire mission, 2012–2019 (Baker et al., 2014; Claudepierre et al., 2019; W. Li et al., 2015; X. Li et al., 2015). The new electron belt observed by CIRBE clearly demonstrates, Figures 1b and 1c, that >1 MeV electrons penetrated to $L < 1.5$ and >2.5 MeV electrons penetrated to $L < 2.5$ after a more severe geomagnetic storm (the minimal Dst index is around −400 nT), which is also shown with PROBA-V/EPT measurements (Pierrard et al., 2024).
2. Detailed structures of energy spectrum. There are more than 10 energy channels of CIRBE/REPTile-2 for electrons at 1.5–4 MeV while there are 2 and 3 energy channels of RBSP/REPT in the same energy range. Thus, more detailed features of the new electron belt are unveiled by CIRBE's observations.
3. Accompanied by the new proton belt. The new proton belt was observed after the 10 May 2024 storm, which was associated with a solar energetic proton (SEP) event while no new proton belt was reported during previous observed remnant belts of electrons.

3.2. Physical Implications of the Long-Lasting New Electron Radiation Belt

Plasmaspheric Hiss Waves: The scenario for the observations more than 1 month after the super storm is that electrons with all energies up to 5 MeV were enhanced in the slot region ($L \sim 2.5$–3.5) during or right after the storm (e.g., Pierrard et al., 2024). The plasmasphere was pushed into lower L and recovered after the storm, as shown by the black curve in the top panel of Figure 3, thus the enhanced electrons stayed inside plasmasphere. Plasmaspheric hiss interacts with lower energy electrons more efficiently (e.g., Lyons & Thorne, 1973), scattering them into the atmosphere and would have reproduced the slot region as shown in Figure 1b, except that higher energy (>1.3 MeV) electrons in that region are not as affected by plasmaspheric hiss. In quiet periods, no chorus waves or strong EMIC waves are inside the plasmasphere (Halford et al., 2016; W. Li et al., 2016; Saikin et al., 2016; Shi et al., 2019). Thus, these high energy electrons stayed trapped. The inserted diagram of the electrons' lifetimes in Figure 1c is from Claudepierre et al. (2020) calculated by an approximate formula in Albert and Shprits (2009) using pitch angle diffusion coefficients as input:

$$\tau \approx \int_{\alpha_L}^{\pi/2} \frac{1}{2D_{\alpha\alpha}\tan\alpha} d\alpha \tag{1}$$

where τ is electron lifetime, α_L is the equatorial loss cone angle, α is the equatorial pitch angle, $D_{\alpha\alpha}$ is the bounce-averaged pitch angle diffusion coefficient. Figure 4 illustrates how the electron lifetime induced by hiss wave are obtained and explains the formation of the new belt's inner edge. Figure 4a shows an example of the hiss wave amplitudes at $L = 2$–4 given by the empirical model of Spasojevic et al. (2015). Combined with the statistical frequency spectrum of W. Li et al. (2015), and the wave normal angle spectrum from Ni et al. (2013), pitch angle diffusion coefficients are calculated using the "Full Diffusion Code" (Ni et al., 2008; Shprits & Ni, 2009). The calculation results for four selected electron energies (listed in Figure 4c) at $L = 2.5$ are shown in Figure 4b. Close to the bounce loss cone (~11.3° at $L = 2.5$ indicated by the vertical dashed line), pitch angle diffusion coefficients

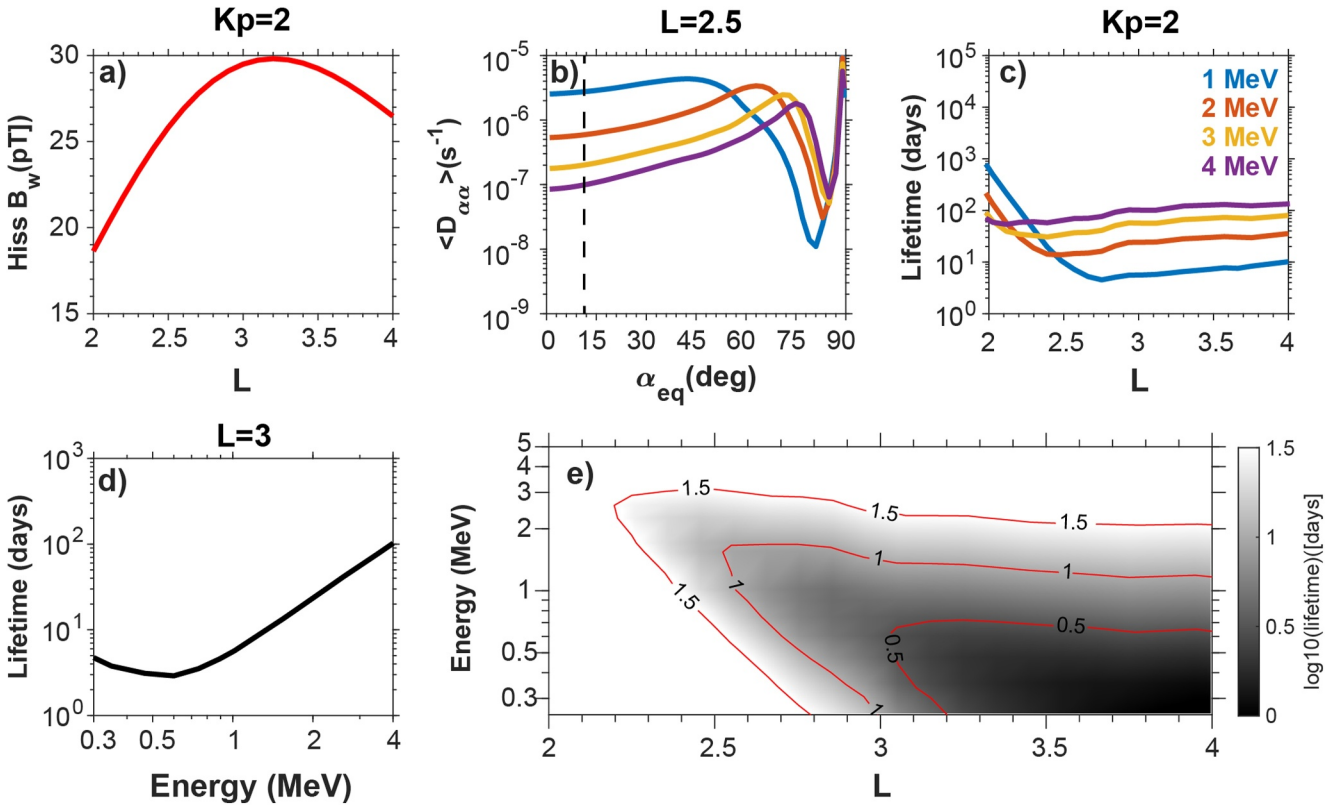

Figure 4. (a) Wave amplitude of hiss waves as a function of L when Kp = 2 given by the Spasojevic et al. (2015) model. (b) Calculation results of bounce-averaged pitch angle diffusion coefficients induce by hiss waves for four selected electron energies at L = 2.5. (c) Lifetime of electrons scattered by hiss waves as a function of L. (d) Lifetime of electrons as a function of energies at L = 3. (e) The same lifetime of electrons inserted in Figure 1c but now re-plotted as a function of L and energies, including three contours of constant lifetime (in log10 [days]).

decrease as electron energies increase from 1 to 4 MeV. Based on Equation 1, we can find that pitch angle diffusion coefficients close to the bounce loss cone (larger $\frac{1}{\tan\alpha}$ values) contribute more to electron lifetime. As a result, 1 MeV electrons have the shortest lifetime due to the larger pitch angle diffusion coefficients near the loss cone, while 4 MeV electrons have the longest lifetime, as shown in Figure 4c. At $L > 2.5$, 1 MeV electrons have the shortest lifetime while the electron energies corresponding to the shortest lifetime shift to higher electron energies at $L < 2.5$. For example, lifetimes of 2 MeV electrons change to shorter than 1 MeV electrons at $L \approx 2.4$ since the electron energies interacted with hiss waves increase as L values decrease (Summers et al., 2007; Zhao et al., 2019). The energy and L-dependence scattering effects induced by hiss waves leads to the sloped upper boundary of inner belt electrons (e.g., Reeves et al., 2016). The lifetimes of electrons (Figure 4c) in the new belt (1.3–5 MeV electrons) due to hiss wave scattering are mostly above 30 days. That is why the new belt showed only a slight variation from 6/17 (Figure 1b) to 6/20 (Figure 1c). This example shows that the lifetimes of relativistic electrons depend on their energy and the local plasma density and magnetic field strength. However, after another magnetic storm on 6/28 the plasmapause likely fell below L = 3.5. Other waves, for example, EMIC and chorus waves, or enhanced hiss waves may have scattered electrons in the new belt (e.g., Blum et al., 2015; Breneman et al., 2017; Chen et al., 2022; Hogan et al., 2021; Z. Li et al., 2014) leading to their decay as shown in Figure 1d. Previous studies also use energy-dependent scattering effects by hiss waves to explain the slow decay of remnant belts (Thorne et al., 2013). However, the L range of previously reported remnant belts (generally at $L > 3$) is higher than the new electron belt reported in this study. Thanks to the high-energy-resolution of CIRBE/REPTile-2, the consistency between hiss-induced electron lifetime contours and energy-dependent boundaries of the inner electron belt as well as boundaries of the remnant belts are clearly present, as shown in Figure 1c, which is re-plotted as Figure 4e, enlarged and including the contours of lifetime for different energy and L. Lifetime of electrons as a function of energies at L = 3 is shown in Figure 4d.

Radial diffusion: We have also investigated the phase space density (PSD) radial gradient for the new belt electrons (see Figure A1 in Appendix A) to determine if radial diffusion plays a significant role in preserving or causing their decay. Since CIRBE is in a LEO, it only measures electrons mirroring at or below its position, The field of view (51°) of REPTile-2 is ensured to point perpendicularly to the local magnetic field by an active attitude control system (X. Li et al., 2022; X. Li, Selesnick, et al., 2024). Assuming that the measured electrons are mirroring at CIRBE's position (a reasonable assumption), the electrons measured at different L have different equatorial pitch angle. To see the PSD for a given first and second adiabatic invariants, μ and K, we have assumed an equatorial pitch angle distribution (PAD) of sin (α), where α is the corresponding equatorial pitch angle, based on statistical study (e.g., Gannon et al., 2007; Zhao et al., 2018). Then we extrapolated the electron flux measured by REPTile-2 to the electron flux corresponding to a constant $K = 0.97$ ($G^{1/2}R_E$) (which is shown in Figure A2 in Appendix A) and various μ, for example, 80, 100, 150, 240 MeV/G that covers the energy between 1.3 and 5 MeV in the new belt. We found that the PSD radial profile is rather flat between $L = 2.8$–4, with some slight positive radial gradient at $L \sim 4$ for lower μ (50–100 MeV/G) but flat for higher μ (150–240 MeV/G) (as shown in Figure A3 in Appendix A). There is a stronger radial gradient for all μ at lower $L \sim 2.5$–2.8. Thus, we conclude that radial diffusion is negligible as there are very few perturbations, such as ULF waves, at lower L (~2.5–2.8); normally there are more perturbations at higher L (~4); however, the PSD radial gradient there is small and even slightly positive for lower μ (80–100 MeV/G).

3.3. Space Weather Effects of the Long-Lasting New Radiation Belts

CIRBE/REPTile-2 only measured the "tip of the iceberg" or a fraction of the new radiation belts. Most of them mirror at altitudes above CIRBE's position with larger equatorial pitch angles. Some spacecraft to be placed in geostationary orbit (GEO) are first placed in a geo-transfer-orbit (GTO) and then use electric propulsion to increase their orbit to GEO (Horne & Pitchford, 2015). This process, which can take many months, will expose the spacecraft to the newly produced MeV electrons and protons in the inner belt and slot region for an extended period. The new belts likely increase the total radiation dose accumulated by spacecraft and could damage specific parts of a spacecraft, for example, satellites' solar cells would suffer more radiation damage due to the new proton radiation belt (Horne & Pitchford, 2015). However, further calculations are needed to quantify the exact effects of the new electron and proton belt on spacecraft in GTO orbit.

4. Summary

Thanks to the high-energy-resolution measurements of REPTile-2 onboard CIRBE, a new electron belt and new proton belt were identified, even though CIRBE did not resume measurements until over a month after these new belts were created. The physical processes creating these belts are to be further investigated, which is beyond the scope of this paper. The persistence of the new electron belt (1.3–5 MeV) around $L = 2.5$–3.5 provides a good case for investigating their lifetimes due to interactions with plasma hiss waves as a function of energy, local plasma density, and magnetic field strength, as demonstrated by the inserted diagram in the slot region in Figures 1c and 4 showing the calculated lifetimes due to interaction with plasma hiss waves. The significant decay after another storm (on 6/28) also provides a good case study for investigating other wave-particle interactions, such as EMIC and chorus waves that scatter high energy electrons into the atmosphere, which will be investigated in the future. The stability of the new proton belt is consistent with current understanding that their loss is mainly due to collisions with free and bound electrons, which is not significant over the observed period. Thus, the new proton belt is expected to last much longer, perhaps over a year.

Appendix A

Here we present the processes of calculating the phase space density (PSD) radial gradient for the new belt electrons, 1.3–5 MeV at $L \sim 2.5$–3.5. Since PSD is defined as a function of three adiabatic invariants, L^* related to the third adiabatic invariant Φ ($L^* = \frac{2\pi M}{|\Phi| R_E}$) is used to describe PSD. The difference between L^* and L (i.e., used in the main text) is less than 0.01 for $L < 4$ at CIRBE's orbits. To calculate the PSD, based on measurements from CIRBE, we extrapolate electron fluxes to pitch angles corresponding to a fixed K value, where $K = \int_{s_m}^{s'_m} \sqrt{B_m - B(s)}\, ds$, based on an assumption of the electron equatorial pitch angle distribution. Then PSD is calculated by $f(\mu, K, L^*) = \frac{j(E, \alpha_{eq}, L)}{P^2}$, where P is the particle momentum, E is particle energy, $\mu = \frac{P_\perp^2}{2 m_0 B}$, and M is

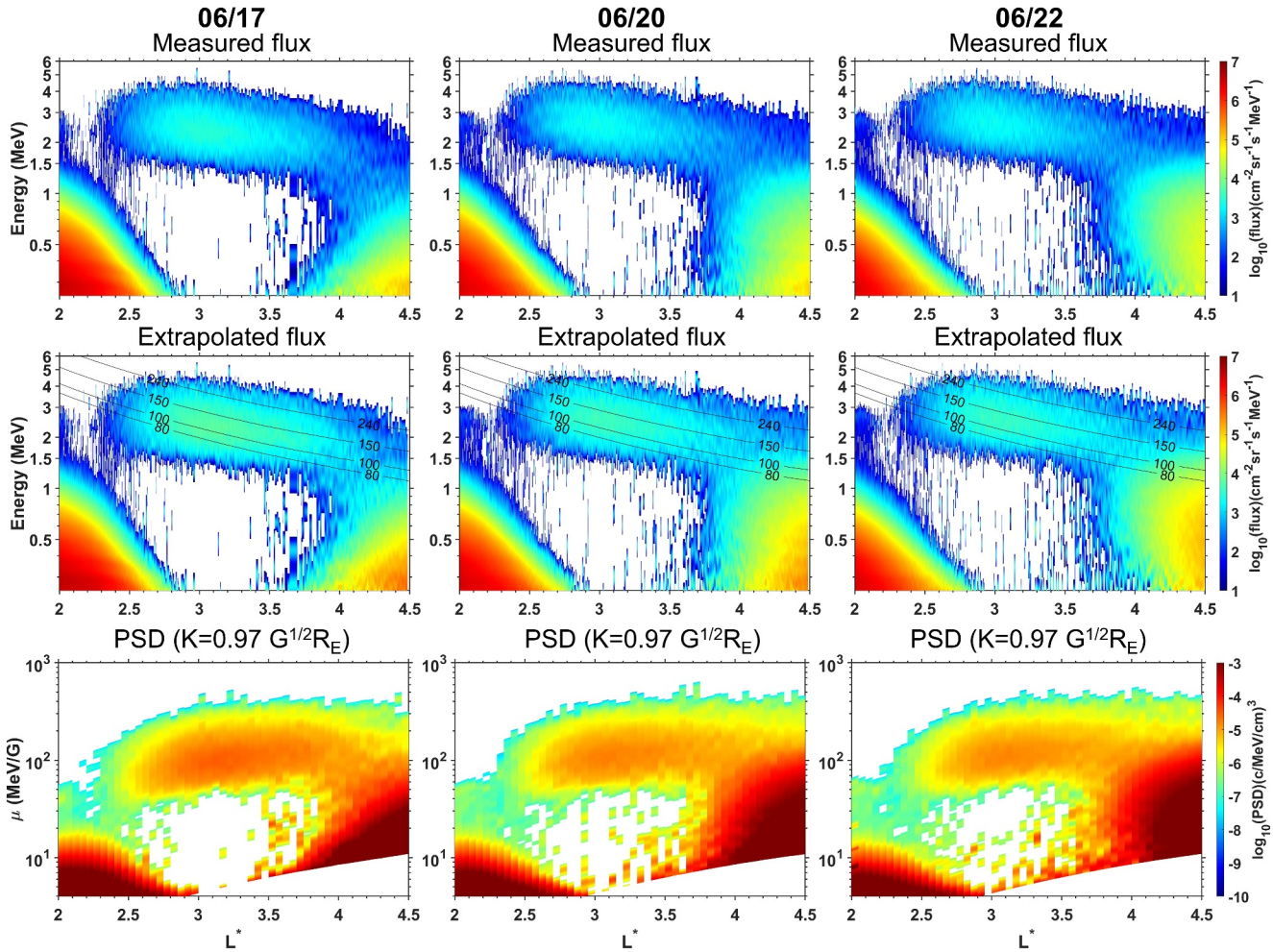

Figure A1. (top row) color-coded logarithmic electron fluxes measured by CIRBE in the L^* region from 2 to 4.5, where the new electron belt is included during the same pass on 6/17 and 6/20 as shown in Figures 1b and 1c, and a similar pass on 6/22; (middle row) extrapolated electron fluxes to equatorial pitch angles corresponding to a constant $K = 0.97\ G^{1/2}R_E$ (see Figure A2) during the three passes. Dashed curves represent the contours of μ = 80, 100, 150, and 240 MeV/G; (bottom row) calculated phase space density of electrons based on CIRBE measurements and extrapolation in equatorial pitch angle for the fixed K as a function of μ and L^*.

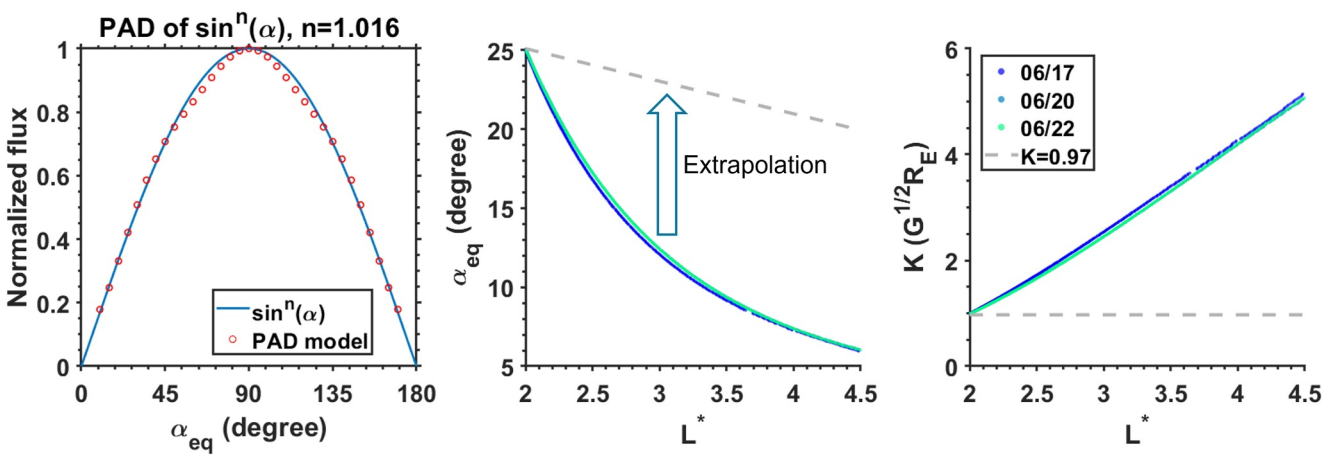

Figure A2. Electron flux extrapolations based on a pitch angle distribution assumption. (left) the assumed equatorial pitch angle distribution by $\sin^n(\alpha)$, where $n = 1.016$, fitting the empirical PAD model (Zhao et al., 2018); (middle) corresponding equatorial pitch angles at different L^* during the three passes. The gray dashed line marks the pitch angles extrapolated to for the fixed K ($0.97\ G^{1/2}R_E$); (right) corresponding K at different L^* during the three passes. The gray dashed line is at the fixed K value for extrapolation.

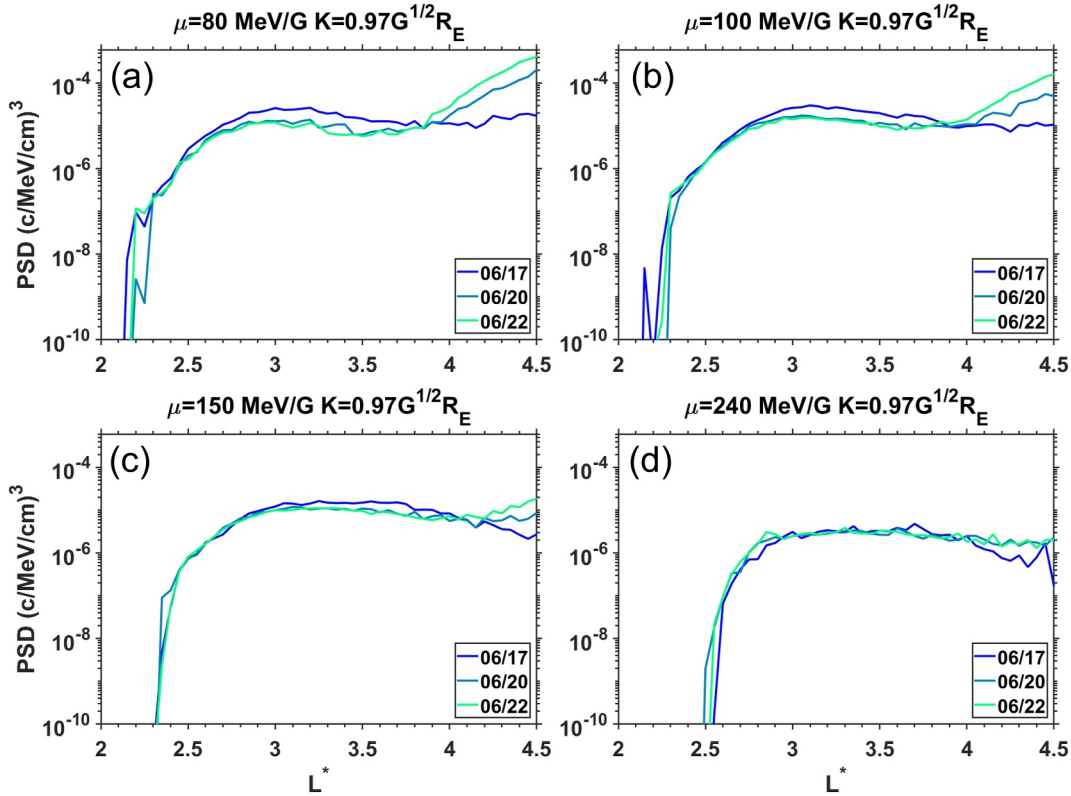

Figure A3. PSD radial profile at the selected μ during the three passes on 6/17, 6/20, and 6/22.

the Earth's dipole magnetic moment. For this study, K and L^* are calculated based on the IGRF magnetic field model. Figure A1 shows the measured flux, extrapolated flux (applied to the flux at all energies), and calculated PSD for the new electron belt. Figure A2 displays the assumption of pitch angle distribution and the process of extrapolation for a fixed K. Figure A3 shows the PSD radial profile of the new belt electrons from three indicated passes.

Data Availability Statement

CIRBE/REPTile-2 data used to generate all figures can be accessed from X. Li, Xiang, et al. (2024).

Acknowledgments
We thank the entire CIRBE team. The CIRBE mission operation team which downloaded and processed the raw data from CIRBE. We thank Dr. Richard Selesnick, Dr. Shawn Young, Dr. W. R. Johnston, Dr. Jay Albert, Dr. Howard Singer, Dr. Mary K. Hudson, and David Pitchford for their helpful discussions. We also thank Nation Central University of Taiwan and NASA/Wallops Flight Facility for their help to download some of the CIRBE data. This work was supported by NASA Grants 80NSSC18K1276 (H-FORT) and 80NSSC21K0583, and NSF Grant AGS 2348553.

References

Albert, J. M., & Ginet, G. P. (1998). CRRES observations of radiation belt protons 2. Time-dependent radial diffusion. *Journal of Geophysical Research*, *103*(A7), 14865–14878. https://doi.org/10.1029/98JA00290

Albert, J. M., Ginet, G. P., & Gussenhoven, M. S. (1998). CRRES observations of radiation belt protons 1. Data overview and steady state radial diffusion. *Journal of Geophysical Research*, *103*(A5), 9261–9274. https://doi.org/10.1029/97JA02869

Albert, J. M., & Shprits, Y. Y. (2009). Estimates of lifetimes against pitch angle diffusion. *Journal of Atmospheric and Solar-Terrestrial Physics*, *71*(16), 1647–1652. https://doi.org/10.1016/j.jastp.2008.07.004

Baker, D. N., Hoxie, V., Zhao, H., Jaynes, A. N., Kanekal, S., Li, X., & Elkington, S. (2019). Multiyear measurements of radiation belt electrons: Acceleration, transport, and loss. *Journal of Geophysical Research: Space Physics*, *124*(4), 2588–2602. https://doi.org/10.1029/2018JA026259

Baker, D. N., Jaynes, A. N., Hoxie, V. C., Thorne, R. M., Foster, J. C., Li, X., et al. (2014). An impenetrable barrier to ultrarelativistic electrons in the Van Allen radiation belts. *Nature*, *515*(7528), 531–534. https://doi.org/10.1038/nature13956

Baker, D. N., Kanekal, S. G., Hoxie, V. C., Henderson, M. G., Li, X., Spence, H. E., et al. (2013). A long-lived relativistic electron storage ring embedded in Earth's outer Van Allen belt. *Science*, *340*(6129), 186–190. https://doi.org/10.1126/science.1233518

Baker, D. N., Kanekal, S. G., Li, X., Monk, S. P., Goldstein, J., & Burch, J. L. (2004). An extreme distortion of the Van Allen belt arising from the "Halloween" solar storm in 2003. *Nature*, *432*(7019), 878–881. https://doi.org/10.1038/nature03116

Blum, L. W., Halford, A., Millan, R., Bonnell, J. W., Goldstein, J., Usanova, M., et al. (2015). Observations of coincident EMIC wave activity and duskside energetic electron precipitation on 18–19 January 2013. *Geophysical Research Letters*, *42*(14), 5727–5735. https://doi.org/10.1002/2015GL065245

Breneman, A. W., Crew, A., Sample, J., Klumpar, D., Johnson, A., Agapitov, O., et al. (2017). Observations directly linking relativistic elec-tron microbursts to whistler mode chorus: Van Allen Probes and FIREBIRD II. *Geophysical Research Letters*, *44*(22), 11265–11272. https://doi.org/10.1002/2017GL075001

Chen, L., Zhang, X.-J., Artemyev, A., Angelopoulos, V., Tsai, E., Wilkins, C., & Horne, R. B. (2022). Ducted chorus waves cause sub-relativistic and relativistic electron microbursts. *Geophysical Research Letters*, *49*(5), e2021GL097559. https://doi.org/10.1029/2021GL097559

Claudepierre, S. G., Ma, Q., Bortnik, J., O'Brien, T. P., Fennell, J. F., & Blake, J. B. (2020). Empirically estimated electron lifetimes in the Earth's radiation belts: Comparison with theory. *Geophysical Research Letters*, *47*(3), e2019GL086056. https://doi.org/10.1029/2019GL086056

Claudepierre, S. G., O'Brien, T. P., Looper, M. D., Blake, J. B., Fennell, J. F., Roeder, J. L., et al. (2019). A revised look at relativistic electrons in the Earth's inner radiation zone and slot region. *Journal of Geophysical Research: Space Physics*, *124*(2), 934–951. https://doi.org/10.1029/2018JA026349

Engel, M., Kress, B., Hudson, M., & Selesnick, R. (2016). Comparison of Van Allen Probes radiation belt proton data with test particle simulation for the 17 March 2015 storm. *Journal of Geophysical Research: Space Physics*, *121*(11), 11–035. https://doi.org/10.1002/2016ja023333

Evans, D. S., & Greer, M. S. (2004). *Polar orbiting environmental satellite space environment monitor-2: Instrument descriptions and archive data documentation archive data documentation, NOAA technical Memorandum 93, version 1.4*. Space Weather Predict. Cent.

Gannon, J., Li, X., & Heynderickx, D. (2007). Pitch angle distribution analysis of radiation belt electrons based on combined release and radiation effects satellite medium electrons a data. *Journal of Geophysical Research*, *112*(A5). https://doi.org/10.1029/2005ja011565

Halford, A. J., Fraser, B. J., Morley, S. K., Elkington, S. R., & Chan, A. A. (2016). Dependence of EMIC wave parameters during quiet, geomagnetic storm, and geomagnetic storm phase times. *Journal of Geophysical Research: Space Physics*, *121*(7), 6277–6291. https://doi.org/10.1002/2016JA022694

Hogan, B., Li, X., Zhao, H., Khoo, L., Jaynes, A., Kanekal, S., & Baker, D. N. (2021). Multi-MeV electron dynamics near the inner edge of the outer radiation belt. *Geophysical Research Letters*, *48*(23), e2021GL095455. https://doi.org/10.1029/2021GL095455

Horne, R. B., & Pitchford, D. (2015). Space weather concerns for all-electric propulsion satellites. *Space Weather*, *13*(8), 430–433. https://doi.org/10.1002/2015SW001198

Khoo, L.-Y., Li, X., Selesnick, R. S., Schiller, Q., Zhang, K., Zhao, H., et al. (2022). On the challenges of measuring energetic particles in the inner belt: A Geant4 simulation of an energetic particle detector instrument, REPTile-2. *Journal of Geophysical Research: Space Physics*, *127*(4), e2021JA030249. https://doi.org/10.1029/2021JA030249

Li, W., & Hudson, M. K. (2019). Earth's Van Allen radiation belts: From discovery to the Van Allen Probes era. *Journal of Geophysical Research: Space Physics*, *124*(11), 8319–8351. https://doi.org/10.1029/2018JA025940

Li, W., Ma, Q., Thorne, R. M., Bortnik, J., Kletzing, C. A., Kurth, W. S., et al. (2015). Statistical properties of plasmaspheric hiss derived from Van Allen Probes data and their effects on radiation belt electron dynamics. *Journal of Geophysical Research: Space Physics*, *120*(5), 3393–3405. https://doi.org/10.1002/2015JA021048

Li, W., Santolik, O., Bortnik, J., Thorne, R. M., Kletzing, C. A., Kurth, W. S., & Hospodarsky, G. B. (2016). New chorus wave properties near the equator from Van Allen Probes wave observations. *Geophysical Research Letters*, *43*(10), 4725–4735. https://doi.org/10.1002/2016GL068780

Li, X. (2024). Unveiling energetic particle dynamics in the near-Earth environment from CubeSat missions. *AGU Advances*, *5*(3), e2024AV001256. https://doi.org/10.1029/2024AV001256

Li, X., Baker, D. N., Temerin, M., Cayton, T. E., Reeves, G. D., Selesnick, R. S., et al. (1999). Rapid enhancements of relativistic electrons deep in the magnetosphere during the May 15, 1997, magnetic storm. *Journal of Geophysical Research*, *104*(A3), 4467–4476. https://doi.org/10.1029/1998JA900092

Li, X., Kohnert, R., Palo, S., Selesnick, R., Khoo, L., & Schiller, Q. (2022). Two generations of CubeSat missions (CSSWE and CIRBE) to take on the challenges of measuring relativistic electrons in Earth's magnetosphere. In *36th Annual Small Satellite Conference*. Retrieved from https://digitalcommons.usu.edu/cgi/viewcontent.cgi?article=5311&context=smallsat

Li, X., Oh, K. S., & Temerin, M. (2007). Prediction of the AL index using solar wind parameters. *Journal of Geophysical Research*, *112*(A6), A06224. https://doi.org/10.1029/2006JA011918

Li, X., Selesnick, R., Mei, Y., O'Brien, D., Hogan, B., Xiang, Z., et al. (2024). First results from REPTile-2 measurements onboard CIRBE. *Geophysical Research Letters*, *51*(3), e2023GL107521. https://doi.org/10.1029/2023GL107521

Li, X., Selesnick, R. S., Baker, D. N., Jaynes, A. N., Kanekal, S. G., Schiller, Q., et al. (2015). Upper limit on the inner radiation belt MeV electron intensity. *Journal of Geophysical Research: Space Physics*, *120*(2), 1215–1228. https://doi.org/10.1002/2014JA020777

Li, X., & Temerin, M. (2001). The electron radiation belt. *Space Science Reviews*, *96*(12). https://doi.org/10.1023/A:1005221108016

Li, X., Xiang, Z., Mei, Y., O'Brien, D., Brennan, D., Zhao, H., et al. (2024). A new electron and proton radiation belt identified by CIRBE/REPTile-2 measurements after the magnetic super storm of May 10, 2024 [Dataset]. *Figshare*. https://doi.org/10.6084/m9.figshare.26521360.v1

Li, Z., Engel, M., Hudson, M., Kress, B., Patel, M., & Selesnick, R. (2024). The Impact of the 8–10 March 2012 geomagnetic storm on inner zone protons as measured by Van Allen Probes. *Journal of Geophysical Research: Space Physics*, *129*(10), e2024JA032800. https://doi.org/10.1029/2024JA032800

Li, Z., Millan, R. M., Hudson, M. K., Woodger, L. A., Smith, D. M., Chen, Y., et al. (2014). Investigation of EMIC wave scattering as the cause for the BARREL 17 January 2013 relativistic electron precipitation event: A quantitative comparison of simulation with observations. *Geophysical Research Letters*, *41*(24), 8722–8729. https://doi.org/10.1002/2014GL062273

Luo, B., Li, X., Temerin, M., & Liu, S. (2013). Prediction of the AU, AL, and AE indices using solar wind parameters. *Journal of Geophysical Research: Space Physics*, *118*(12), 7683–7694. https://doi.org/10.1002/2013JA019188

Lyons, L. R., & Thorne, R. M. (1973). Equilibrium structure of radiation belt electrons. *Journal of Geophysical Research*, *78*(13), 2142–2149. https://doi.org/10.1029/JA078i013p02142

Mei, Y., Li, X., O'Brien, D., Xiang, Z., Zhao, H., Sarris, T., et al. (2025). Characteristics of "zebra stripes" of relativistic electrons unveiled by CIRBE/REPTile-2 measurements and test particle simulations. *Journal of Geophysical Research: Space Physics*, *130*, e2024JA033187. https://doi.org/10.1029/2024JA033187

Ni, B., Bortnik, J., Thorne, R. M., Ma, Q., & Chen, L. (2013). Resonant scattering and resultant pitch angle evolution of relativistic electrons by plasmaspheric hiss. *Journal of Geophysical Research: Space Physics*, *118*(12), 7740–7751. https://doi.org/10.1002/2013JA019260

Ni, B., Thorne, R. M., Shprits, Y. Y., & Bortnik, J. (2008). Resonant scattering of plasma sheet electrons by whistler-mode chorus: Contribution to diffuse auroral precipitation. *Geophysical Research Letters*, *35*(11), L11106. https://doi.org/10.1029/2008GL034032

O'Brien, T. P., & Moldwin, M. B. (2003). Empirical plasmapause models from magnetic indices. *Geophysical Research Letters*, *30*(4), 1152. https://doi.org/10.1029/2002GL016007

Pierrard, V., Winant, A., Botek, E., & Péters de Bonhome, M. (2024). The Mother's Day solar storm of 11 May 2024 and its effect on Earth's radiation belts. *Universe*, *10*, 391. https://doi.org/10.3390/universe10100391

Reeves, G. D., Friedel, R. H. W., Larsen, B. A., Skoug, R. M., Funsten, H. O., Claudepierre, S. G., et al. (2016). Energy dependent dynamics of keV to MeV electrons in the inner zone, outer zone, and slot regions. *Journal of Geophysical Research: Space Physics*, *121*(1), 397–412. https://doi.org/10.1002/2015JA021569

Saikin, A. A., Zhang, J.-C., Smith, C. W., Spence, H. E., Torbert, R. B., & Kletzing, C. A. (2016). The dependence on geomagnetic conditions and solar wind dynamic pressure of the spatial distributions of EMIC waves observed by the Van Allen Probes. *Journal of Geophysical Research: Space Physics*, *121*(5), 4362–4377. https://doi.org/10.1002/2016JA022523

Selesnick, R. S., Baker, D. N., Jaynes, A. N., Li, X., Kanekal, S. G., Hudson, M. K., & Kress, B. T. (2016). Inward diffusion and loss of radiation belt protons. *Journal of Geophysical Research: Space Physics*, *121*(3), 1969–1978. https://doi.org/10.1002/2015JA022154

Selesnick, R. S., Baker, D. N., Kanekal, S. G., Hoxie, V. C., & Li, X. (2018). Modeling the proton radiation belt with Van Allen Probes relativistic electron-proton telescope data. *Journal of Geophysical Research: Space Physics*, *123*(1), 685–697. https://doi.org/10.1002/2017JA024661

Selesnick, R. S., & Looper, M. D. (2023). Field-line curvature scattering at the outer boundary of the proton radiation belt. *Journal of Geophysical Research: Space Physics*, *128*(7), e2023JA031509. https://doi.org/10.1029/2023JA031509

Selesnick, R. S., Looper, M. D., & Mewaldt, R. A. (2007). A theoretical model of the inner proton radiation belt. *Space Weather*, *5*(4), S04003. https://doi.org/10.1029/2006SW000275

Sergeev, V., & Tsyganenko, N. (1982). Energetic particle losses and trapping boundaries as deduced from calculations with a realistic magnetic field model. *Planetary and Space Science*, *30*(10), 999–1006. https://doi.org/10.1016/0032-0633(82)90149-0

Shi, R., Li, W., Ma, Q., Green, A., Kletzing, C. A., Kurth, W. S., et al. (2019). Properties of whistler mode waves in Earth's plasmasphere and plumes. *Journal of Geophysical Research: Space Physics*, *124*(2), 1035–1051. https://doi.org/10.1029/2018JA026041

Shprits, Y. Y., & Ni, B. (2009). Dependence of the quasi-linear scattering rates on the wave normal distribution of chorus waves. *Journal of Geophysical Research*, *114*(A11), A11205. https://doi.org/10.1029/2009JA014223

Spasojevic, M., Shprits, Y. Y., & Orlova, K. (2015). Global empirical models of plasmaspheric hiss using Van Allen Probes. *Journal of Geophysical Research: Space Physics*, *120*(12), 10370–10383. https://doi.org/10.1002/2015JA021803

Summers, D., Ni, B., & Meredith, N. P. (2007). Timescales for radiation belt electron acceleration and loss due to resonant wave-particle interactions: 1. Theory. *Journal of Geophysical Research*, *112*(A4), A04206. https://doi.org/10.1029/2006JA011801

Tarantola, A. (2005). *Inverse problem theory and methods for model parameter estimation*. Society for Industrial and Applied Mathematics.

Tarantola, A., & Valette, B. (1982). Generalized nonlinear inverse problems solved using the least squares criterion. *Reviews of Geophysics*, *20*(2), 219–232. https://doi.org/10.1029/RG020i002p00219

Temerin, M., & Li, X. (2006). Dst model for 1995–2002. *Journal of Geophysical Research*, *111*(A4), A04221. https://doi.org/10.1029/2005JA011257

Thorne, R. M., Li, W., Ni, B., Ma, Q., Bortnik, J., Baker, D. N., et al. (2013). Evolution and slow decay of an unusual narrow ring of relativistic electrons near L ∼ 3.2 following the September 2012 magnetic storm. *Geophysical Research Letters*, *40*(14), 3507–3511. https://doi.org/10.1002/grl.50627

Tu, W., Cowee, M. M., & Liu, K. (2014). Modeling the loss of inner belt protons by magnetic field line curvature scattering. *Journal of Geophysical Research: Space Physics*, *119*(7), 5638–5650. https://doi.org/10.1002/2014JA019864

Young, S. L., Denton, R. E., Anderson, B. J., & Hudson, M. K. (2002). Empirical model for μ scattering caused by field line curvature in a realistic magnetosphere. *Journal of Geophysical Research*, *107*(A6), 1069. https://doi.org/10.1029/2000JA000294

Young, S. L., Denton, R. E., Anderson, B. J., & Hudson, M. K. (2008). Magnetic field line curvature induced pitch angle diffusion in the inner magnetosphere. *Journal of Geophysical Research*, *113*(A3), A03210. https://doi.org/10.1029/2006JA01213

Zhao, H., Friedel, R. H. W., Chen, Y., Reeves, G. D., Baker, D. N., Li, X., et al. (2018). An empirical model of radiation belt electron pitch angle distributions based on Van Allen Probes measurements. *Journal of Geophysical Research: Space Physics*, *123*(5), 3493–3511. https://doi.org/10.1029/2018JA025277

Zhao, H., Ni, B., Li, X., Baker, D. N., Johnston, W. R., Zhang, W., et al. (2019). Plasmaspheric hiss waves generate a reversed energy spectrum of radiation belt electrons. *Nature Physics*, *15*(4), 367–372. https://doi.org/10.1038/s41567-018-0391-6